Theoretical investigation of the origin of the multipeak structure of kinetic-energy-release spectra from charge-resonance-enhanced ionization of H_2^+ in intense laser fields

Haixiang He,[1,2] Ruifeng Lu,[3] Peiyu Zhang,[1] Yahui Guo,[1,2] Keli Han,[1,*] and Guozhong He[1]

[1]*State Key Laboratory of Molecular Reaction Dynamics, Dalian Institute of Chemical Physics, Chinese Academy of Sciences, Dalian 116023, China*

[2]*China and Graduate School of the Chinese Academy of Sciences, Beijing, 10039, China*

[3]*Department of Applied Physics, Nanjing University of Science and Technology, Nanjing 210094, China*

(Received 14 July 2011; revised manuscript received 16 August 2011; published 26 September 2011)

The dynamics of hydrogen molecular ions in intense laser pulses (100 fs, $I = 0.77 \times 10^{14}$ W/cm^2 to 2.5×10^{14} W/cm^2) has been studied, and the kinetic-energy-release spectra of Coulomb explosion channel have been calculated by numerically solving the time-dependent Schrödinger equation. In a recent experiment, a multipeak structure from charge-resonance-enhanced ionization is interpreted by a vibrational "comb" at a critical nuclear distance. We found that the peaks could not be attributed to a single vibrational level but a collective contribution of some typical vibrational states in our calculated Coulomb explosion spectra, and the main peak shifts toward the low-energy region with increasing vibrational level, which is also different from the explanation in that experiment. We have also discussed the proton's kinetic-energy-release spectra for different durations with the same laser intensity.

DOI: 10.1103/PhysRevA.84.033418 PACS number(s): 33.20.Xx

I. INTRODUCTION

A number of experimental and theoretical studies of molecules in intense laser fields have revealed many interesting features in the past few decades [1,2]. In the simplest molecular ion, H_2^+, the external effect of the pulse in the intensity range of these studies (10^{12}–10^{15} W/cm^2) cannot be treated as a perturbation due to the comparable strength of the electron with the nuclei and the laser field. The interpretations of molecular dissociation and ionization dynamics caused by intense laser pulses are mainly based on bond softening (BS) [3] and bond hardening (BH) [4], above-threshold dissociation [5], and charge-resonance-enhanced ionization (CREI) [6]. Experimentally, the details of these mechanisms could be detected by energy-resolved spectra of fragments in an intense field, that is, kinetic-energy-release (KER) spectra, which have been found to be sensitive to the peak intensity, pulse duration, pulse shape, and wavelength of the laser pulse [5,7,8].

In principle, an accurate theoretical description of these dynamics needs to explicitly integrate the time-dependent Schrödinger equation (TDSE). Plenty of theoretical investigations have used the Born-Oppenheimer approximation [9,10], which separates the nuclear motion from the electronic motion. It is hard to get exact results since the intense laser field may influence the Coulomb potential of H_2^+. Thus, a full-dimensional simulation that simultaneously considers the nuclear and electronic dynamics is desired for more accuracy. Because of the high computational consumption of the full-dimensional calculation, reasonable approximations have been adopted in some theoretical studies, such as laser-induced alignment that ignores the molecular rotation of the nuclear motion [11,12], although angular dependences of BS and BH channels have been discussed in a recent paper [13]. Furthermore, only two coordinates are needed to describe the electronic motion because of the cylinder symmetry of H_2^+ [14,15]. In brief, a three-dimensional (3D) TDSE solution is necessary for dynamical investigation related to the experiments.

Based on the time-dependent quantum approaches, a quantitative comparison of theoretical versus experimental results is still a challenge. One of the reasons is that the ion H_2^+ prepared from the neutral molecule H_2 in experiments causes interplay between the ionization and fragmentation steps because of the interaction of the ion with laser field. Moreover, the H_2^+ vibrational population is dependent on intensity, and only the vibrational levels below $\upsilon = 4$ populate with a high-peak-intensity laser pulse [16]. Fortunately, the ionic beams have been produced with a Franck-Condon (FC) distribution in some experiments [7,17], which makes comparison of theory versus experiment possible. Using a high-resolution two-dimensional velocity imaging technique, some peaks in KER spectrum from the Coulomb explosion (CE) channel at low peak intensity of the laser pulses were attributed to single vibrational levels, which assumed that ionization occurs at critical nuclear distance for different vibrational states [7]. However, this model is so coarse that the purpose of the present work is to find the essential dynamics for CE channel. We carried out the quantum dynamics calculations for different initial vibrational states of H_2^+ by solving the 3D TDSE using our accurate quantum dynamics method [18,19].

II. THEORY

The TDSE in the cylindrical polar coordinate system for H_2^+ reads as

$$i\frac{\partial\psi(R,\rho,z,t)}{\partial t} = H(R,\rho,z,t)\psi(R,\rho,z,t), \qquad (1)$$

*klhan@dicp.ac.cn

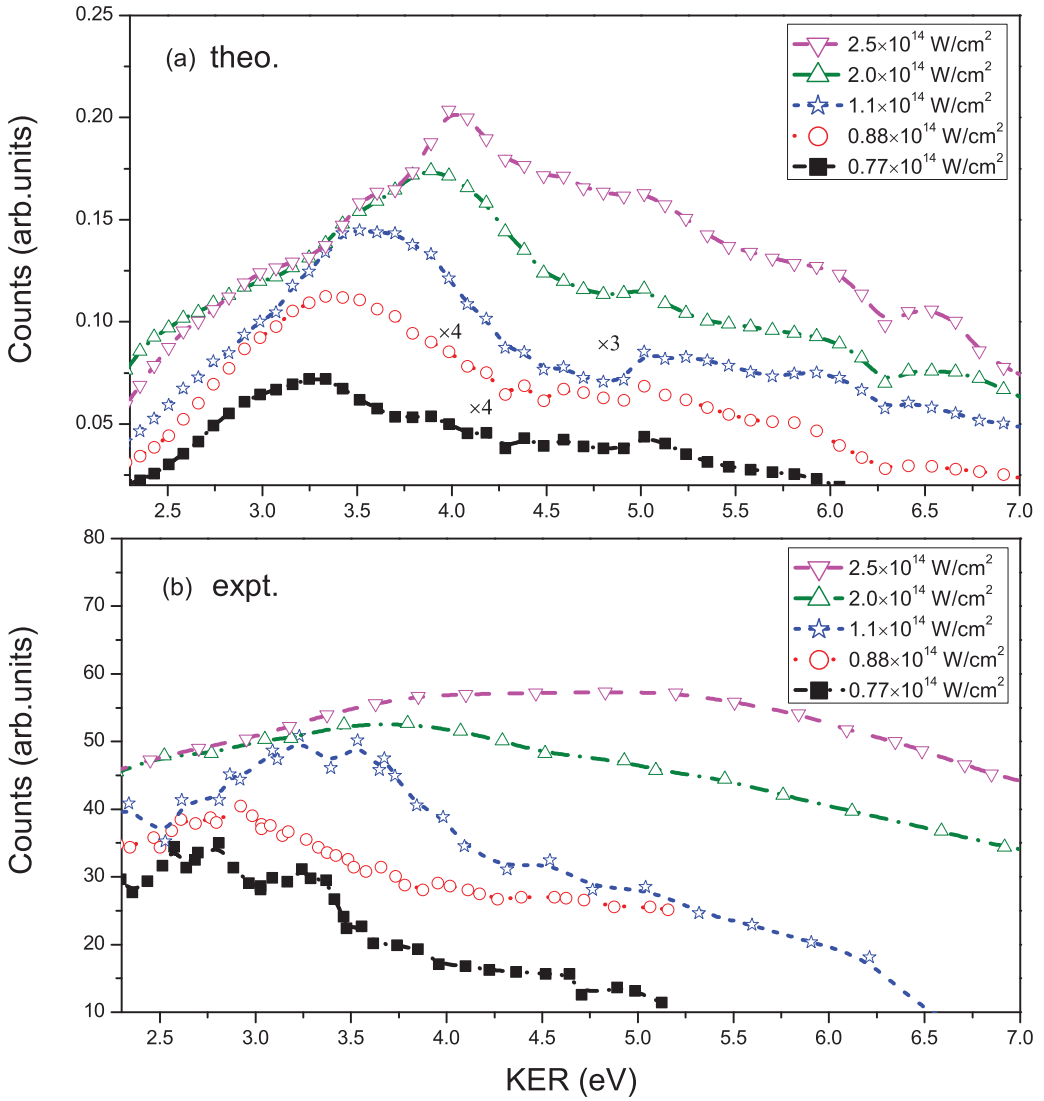

FIG. 1. (Color online) (a) The CE KER spectra for different peak intensities of the pulses (100 fs) vary from 0.77 × 10^{14} W/cm^2 to 2.5 × 10^{14} W/cm^2, corresponding to the experimental data from Ref. [7] shown in panel (b).

where the 3D Hamiltonian in a laser field parallel to the internuclear axis is given by

$$H(R,\rho,z,t) = T_R + T_z + T_\rho + V_c(R,\rho,z) + \kappa z E(t), \quad (2)$$

$$T_R = -\frac{1}{m_p}\frac{\partial^2}{\partial R^2}, \quad (3a)$$

$$T_z = -\frac{2m_p + m_e}{4m_p m_e}\frac{\partial^2}{\partial z^2}, \quad (3b)$$

$$T_\rho = -\frac{2m_p + m_e}{4m_p m_e}\left(\frac{\partial^2}{\partial \rho^2} + \frac{1}{\rho}\frac{\partial}{\partial \rho}\right), \quad (3c)$$

$$V_c(R,\rho,z) = \frac{1}{R} - \frac{1}{[\rho^2 + (z - R/2)^2]^{1/2}} - \frac{1}{[\rho^2 + (z + R/2)^2]^{1/2}}, \quad (4)$$

$$\kappa = 1 + \frac{m_e}{2m_p + m_e}, \quad E(t) = E_0 f(t)\sin(\omega t), \quad (5)$$

where E_0 is the laser peak amplitude, ω is the angular frequency, and $f(t)$ is the envelope of the pulse. In our calculations, Gaussian-shaped 100-fs pulses [with full width at half maximum (FWHM)] of 791 nm wavelength are used, which corresponds to the experiment condition [7]. To solve the above TDSE, we combined the Crank-Nicholson (CN) method in the ρ direction and the sine discrete variable representation (DVR) in the other two directions. The latter is defined as [19]

$$\langle x_i | n \rangle = \sqrt{\frac{2}{L}}\sin(n\pi x_i'/L) = \sqrt{\frac{2}{L}}\sin\left(\frac{in\pi}{N+1}\right), \quad (6)$$

where $L = x_{\max} - x_{\min}$, $x_i' = x_i - x_{\min} = i\Delta x$, $i = 1, 2, \ldots, K$, and $\Delta x = L/(K+1)$. The corresponding DVR basis $|\bar{x}_i\rangle$ is defined as

$$\langle \bar{x}_i \mid n \rangle = \sqrt{\Delta x}\,\langle x_i \mid n \rangle, \quad (7)$$

and the transformation between $|\bar{x}_i\rangle$ and $|n\rangle$ is orthogonal. The flux operator and virtual director methods [20] are employed

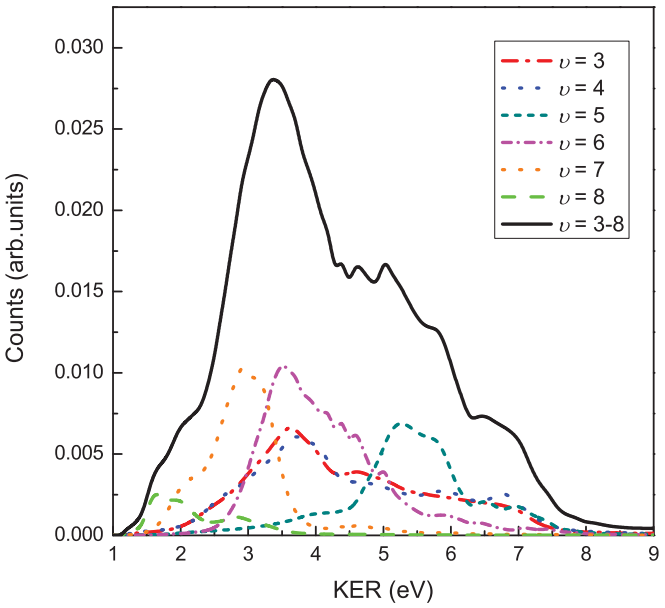

FIG. 2. (Color online) The CE KER spectra for initial vibrational states from $\upsilon = 3$ to $\upsilon = 8$ and the overall kinetic energy distributions (solid black line), which are weighted by the FC factors at the laser intensity of 0.88×10^{14}W/cm^2.

to calculate the probabilities and energy spectra, respectively. A binning procedure is necessary to derive the KER spectra across the whole interaction time of the laser pulse. Atomic units are used throughout the paper.

To economize on computation time, we arrange the time evolution operator to take advantage of the disparity in the time scales of the nuclear and electronic motion, and the resulting operator is

$$e^{-iH\delta t} \approx e^{-iT_R\delta t/2}\left[e^{-iT_z\delta t/(2N)}\left(M_\rho^{\mathrm{CN}}\right)\right.$$
$$\left.\times e^{-i(V_c+kzE(t))\delta t/N} e^{-iT_z\delta t/(2N)}\right]^N e^{-iT_R\delta t/2}. \quad (8)$$

M_ρ^{CN} is the time propagation of ρ direction by the CN method. $N = \sqrt{\mu_N/\mu_e}$, $\mu_N = m_p/2$, and $\mu_e = 2m_p/(2m_p + m_e)$ are the reduced masses of nuclei and electrons, respectively. We tested that $N = 20$ are appropriate. Therefore, the time steps are 0.05 for z and ρ components and 1 for the R component. The grid points for these three coordinates are 450, 30, and 300, respectively. The grids extend up to $|Z|^{\max} = 45$, $\rho^{\max} = 15$, and $R^{\max} = 30$. Absorbing potentials in z, ρ, and R are implemented in order to prevent the reflection of the outgoing wave packets at the borders of the grids.

III. RESULTS AND DISCUSSION

The KER spectra for CE channels with different peak intensities of the pulses (100 fs) are shown in Fig. 1(a). The spectra are obtained by adding up all of the contributions with FC distributions of the states from $\upsilon = 0$ to 9. A multipeak structure is not obviously seen here. The main peak energy shifts from about 3.4 eV to almost 4 eV with the intensity increasing, which is consistent with the experimental data from Ref. [7] in Fig. 1(b). Since the volume effect has not been taken into account in this work, our results could be compared with the experimental results only qualitatively.

Figure 2 shows the KER spectra of CE channel at the intensity of 0.88×10^{14} W/cm^2 for various vibrational states.

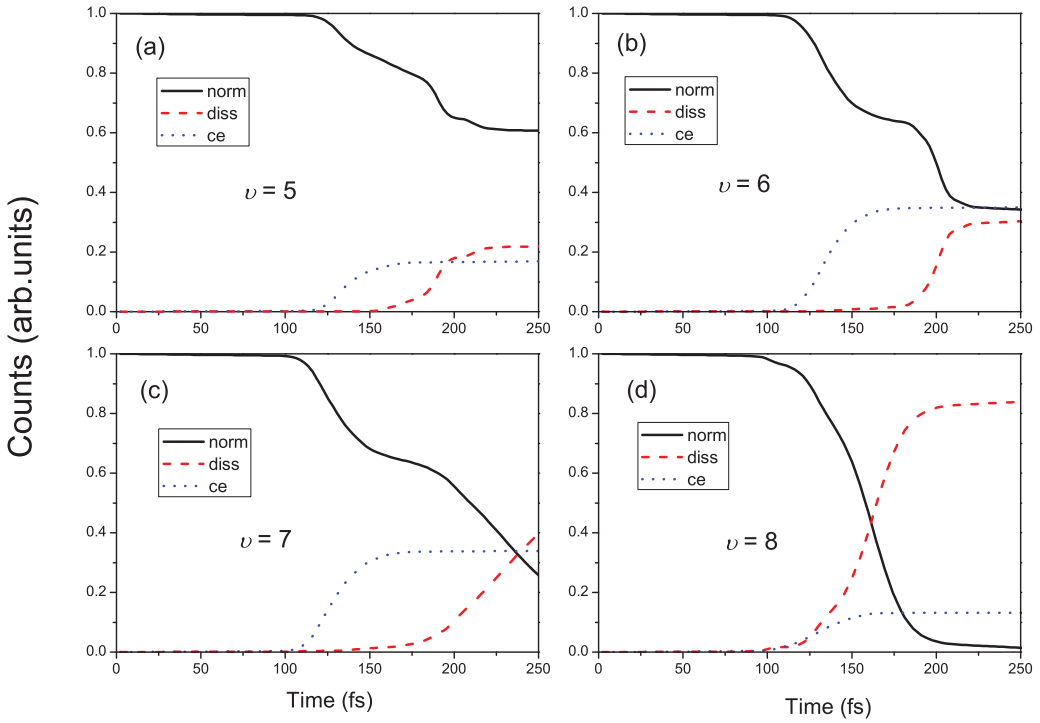

FIG. 3. (Color online) (a)–(d) The norm of the remaining wave packet, the probabilities of dissociation, and CE channels for $\upsilon = 5$,6,7 and 8, respectively. The laser conditions are the same as in Fig. 2.

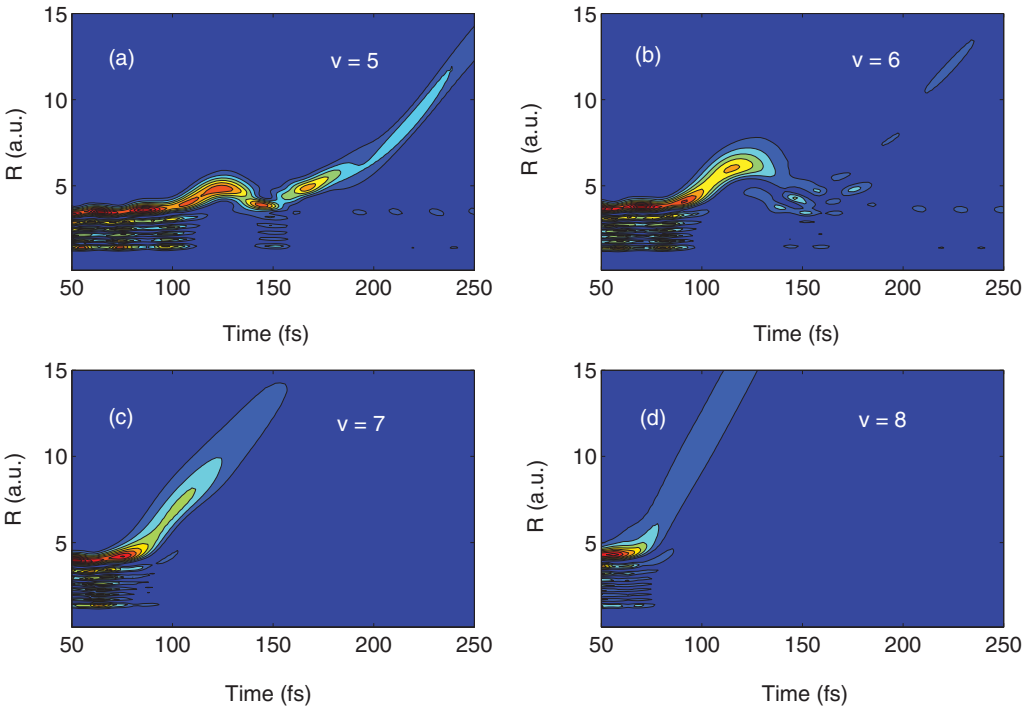

FIG. 4. (Color online) (a)–(d) The time evolution of the nuclear probability density for $\upsilon = 5,6,7$ and 8, respectively.

We depict the CE KER spectra for single vibrational states from $\upsilon = 3$ to 8. The total CE KER spectrum is obtained by adding up all of these contributions with FC distributions of these states. Because of the small ionization probabilities or low weights in FC distributions of some vibrational states (i.e., $\upsilon = 0$, 1, 2, 9, 10, etc.), their contributions could be ignored in this case. The peaks originate from a different mechanism than in the experiment, which attributed

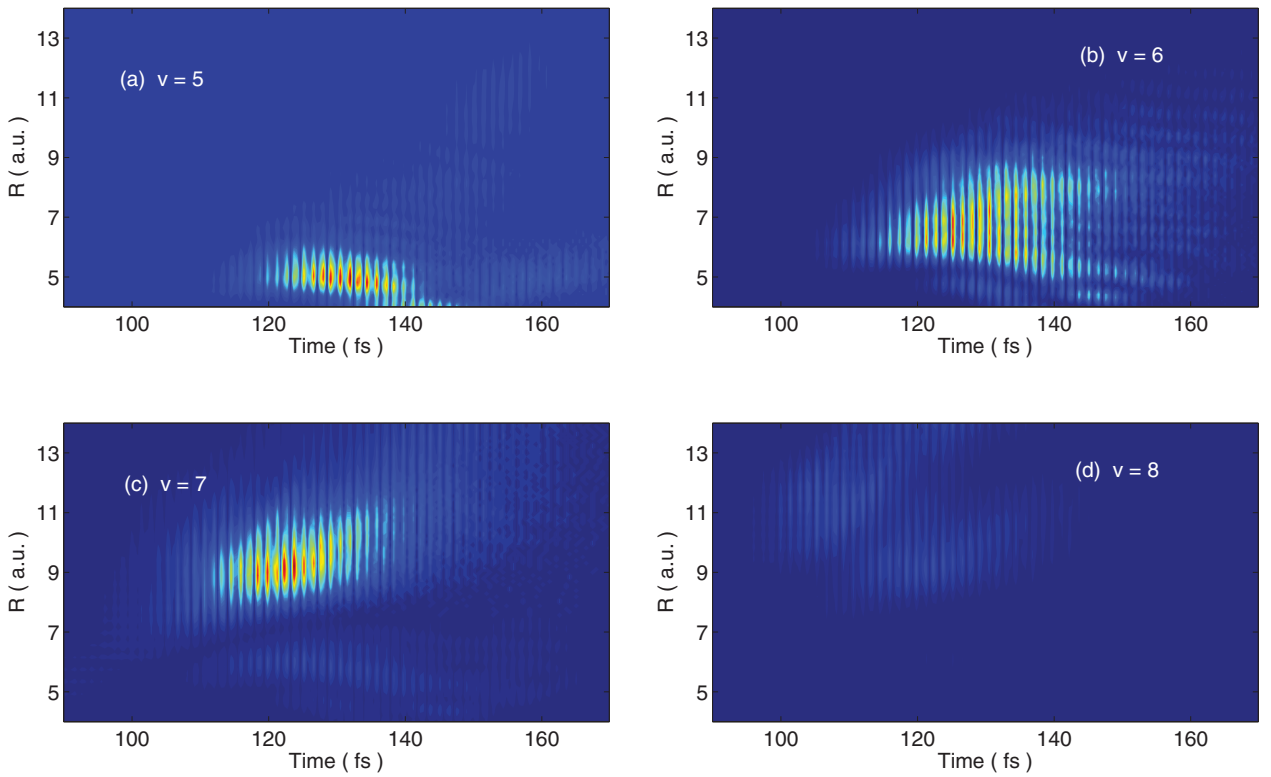

FIG. 5. (Color online) (a-d) The space-time dependent ionization rate for $\upsilon = 5$, 6, 7 and 8.

TABLE I. The nuclear distances (R_{max}) for the main peak of CE channels and their corresponding Coulomb effect energies ($1/R_{max}$) compared with the calculated results (E) for $\upsilon = 5$, 6, 7, and 8.

	R_{max} (a.u.)	$1/R_{max}$ (eV)	E (eV)
$\upsilon = 5$	5.0	5.442	5.347
$\upsilon = 6$	7.2	3.780	3.544
$\upsilon = 7$	9.2	2.958	2.937
$\upsilon = 8$	16.4	1.659	1.665

each peak to a single vibrational state. In our calculations, the peaks cannot be attributed to single states but a collective contribution from all of the states. This is contrary to the explanation of the experiment, which limits the nuclear position for ionization at a large critical internuclear distance about 13 a.u.; therefore, the fragment kinetic energy depends only on the value of binding energy of each vibrational state (E_υ). As we know, as the vibrational state becomes lower, the absolute value of E_υ becomes larger. As a result, the energy of the peak for a single vibrational level increases with increasing vibrational quantum number under the experimental explanation. In our results, however, we can see that the peaks shift toward low energies with the vibrational levels increasing from $\upsilon = 5$ to $\upsilon = 8$. Furthermore, it is irregular for the states $\upsilon = 3$ and $\upsilon = 4$. Next, we discuss this inconsistent phenomenon by comparison with the experimental explanation.

Figure 3 shows the norm of the remaining wave packet and the probabilities for dissociation and CE channels of $\upsilon = 5$, 6, 7, and 8. It indicates that CE processes begin at about 110 fs and end at about 150 fs for these states. Considering the competition between dissociation and ionization, the molecular ion for high vibrational states tends to dissociate rather than to ionize; Fig. 3 shows that the ionization probability decreases with increasing vibrational levels from $\upsilon = 6$. In order to interpret the phenomena described above, we also calculate the time evolution of the nuclear probability density and time-dependent ionization rate of various internuclear distances for each vibrational state in Figs. 4 and 5, respectively. The formula of the nuclear probability density is

$$P(R,t) = \int_{-z_{vd}}^{+z_{vd}} \int_0^{\rho} \rho d\rho dz |\psi(z,R,t)|^2, \qquad (9)$$

where z_{vd} is the border of the z grid, on which the absorbing potential begins to act. Figures 4 and 5 indicate that the molecular ion ionizes at a range of internuclear distance rather than a critical one for all of these states. The scope increases with increasing vibrational level, which is from 3.4 a.u. $< R_c <$ 6.8 a.u. for $\upsilon = 5$ to 5 a.u. $< R_c <$ 27 a.u. for $\upsilon = 8$, and is located at the CREI area. Figures 6(a) and 6(b) show the R-dependent ionization rate for $\upsilon = 5$, 6, 7, and 8 and the total ionization rate added up from $\upsilon = 2$ to $\upsilon = 8$ states after FC averaging, respectively. Figure 6(a) shows that the high vibrational states ionize over a broad R region, which is also reflected in the smooth spectrum in Fig. 2. Two typical peaks located at $R = 5.1$ a.u. and $R = 8.2$ a.u. correspond to proton peak energies of 5.3 eV and 3.3 eV in Fig. 6(b), respectively. Bandrauk *et al.* [21] showed a similar two-peak structure, which is confirmed for the first time in both linearly and circularly polarized pulses, and the enhanced ionization still occurs for nonaligned molecules. The kinetic energy for this channel mostly depends on the Coulomb effect at distances of ionization ($1/R_c$) via dissociative ionization processes. Since the range of distances increases with increasing vibrational level, the kinetic energy shifts lower from $\upsilon = 5$ to $\upsilon = 8$, which is consistent with one-dimensional (1D) quantum dynamics calculations [22]. It is worth noting that a spread in the critical distance ΔR_c of more than 1 a.u. would cause smearing of the contributions from single vibrational levels. The detail of each vibrational state with internuclear distance for the largest ionization probability and its corresponding Coulomb effect energy are shown in Table I, which also presents the energies of the main peaks we calculated in Fig. 2. The energy of the Coulomb effect matches well with the calculated one, which suggests our explanation is reasonable. The situation is different for the case of the lower vibrational levels ($\upsilon = 3$, 4), in which the kinetic energy spectra are almost the same. In this case, ionizations may happen after above-threshold

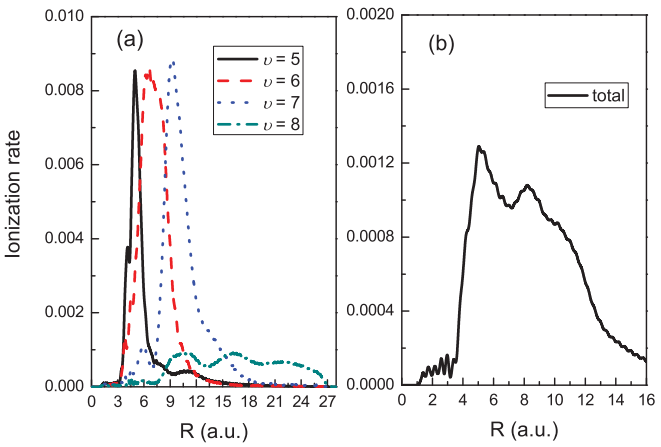

FIG. 6. (Color online) (a) The R-dependent ionization rates for $\upsilon = 5$, 6, 7, and 8 states. (b) The total R-dependent ionization rates from $\upsilon = 2$ to $\upsilon = 8$ states.

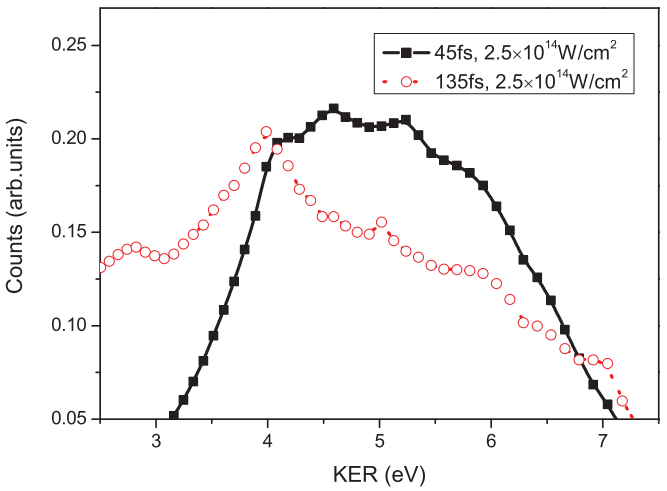

FIG. 7. (Color online) The CE KER spectra for 45 fs and 135 fs with the same laser peak intensity.

dissociation rather than BS process for the higher vibrational levels. For the $\upsilon = 5$ state, the time is shorter to prevent the wave packet from moving further before ionization than that of $\upsilon = 6$ state via BS processes, which means the nuclear distance for CE is smaller than that of higher states but the proton obtains much more energy. The trend can also be observed for other states ($\upsilon = 7, 8$).

We also consider CE KER spectra of different durations of the pulses, which are shown in Fig. 7. It can be seen that as the pulse duration is shorter, the main peak energy becomes greater. For a short pulse (45 fs), which is approaching the vibrational time scale, it may cause a more intensive interference between vibrational states, resulting in smoother spectra than the long pulse (135 fs) with almost the same strength. In contrast, for the 135-fs pulse, the multipeak structure is much more obvious. The peak energy becomes higher with the pulse shortening due to the shorter rising time, making CE at a smaller internuclear distance, which has been observed by Frasinski *et al*. [4].

IV. CONCLUSIONS

To summarize, we have performed a quantum dynamics study of a hydrogen molecular ion in an intense laser field using our LZH-DICP code. With vibrationally resolved CE KER spectra, we found that the peaks could not be attributed to single vibrational levels but originate from the coherent superposition of some typical states, which agrees with the recent 1D result. The energy of the peaks decreases with increasing vibrational levels, and the phenomena are opposite to the explanation of the experiment, in which at a critical nuclear distance they are suspected for CREI. In our calculations, the ionization occurs in a range of nuclear distances, and this plays a much more important role in kinetic energy than the discrepancy of the energy for higher vibrational levels. The two-peak structure of the R-dependent ionization rate for enhanced ionization channel is shown, and each peak is amplified by typical initial vibrational distribution. This indicates the enhanced ionization could be controlled by creating different vibrational states. Also, the main peak energy of CE KER spectra decreases with increasing pulse duration, and a multipeak structure is more obvious for the long pulse.

ACKNOWLEDGEMENT

This work was supported by the NSFC (Grant No. 10974198).

[1] A. Giusti-Suzor, F. H. Mies, L. F. DiMauro, E. Charron, and B. Yang, J. Phys. B **28**, 309 (1995).
[2] J. H. Posthumus, Rep. Prog. Phys. **67**, 623 (2004).
[3] P. H. Bucksbaum, A. Zavriyev, H. G. Muller, and D. W. Schumacher, Phys. Rev. Lett. **64**, 1883 (1990).
[4] L. J. Fransinski, J. H. Posthumus, J. Plumridge, K. Codling, P. F. Taday, and A. J. Langley, Phys. Rev. Lett. **83**, 3625 (1999).
[5] G. Jolicard and O. Atabek, Phys. Rev. A **46**, 5845 (1992).
[6] T. Zuo and A. D. Bandrauk, Phys. Rev. A **52**, R2511 (1995).
[7] D. Pavičić, A. Kiess, T. W. Hänsch, and H. Figger, Phys. Rev. Lett. **94**, 163002 (2005).
[8] K. Sändig, H. Figger, and T. W. Hänsch, Phys. Rev. Lett. **85**, 4876 (2000).
[9] V. Serov, A. Keller, O. Atabek, H. Figger, and D. Pavičić, Phys. Rev. A **72**, 033413 (2005).
[10] P. Q. Wang, A. M. Sayler, K. D. Carnes, J. F. Xia, M. A. Smith, B. D. Esry, and I. Ben-Itzhak, Phys. Rev. A **74**, 043411 (2006).
[11] B. Feuerstein, Th. Ergler, A. Rudenko, K. Zrost, C. D. Schröter, R. Moshammer, J. Ullrich, T. Niederhausen, and U. Thumm, Phys. Rev. Lett. **99**, 153002 (2007).
[12] U. Thumm, T. Niederhausen, and B. Feuerstein, Phys. Rev. A **77**, 063401 (2008).
[13] L. J. Frasinski, J. Plumridge, J. H. Posthumus, K. Codling, P. F. Taday, E. J. Divall, and A. J. Langley, Phys. Rev. Lett. **86**, 2541 (2001).
[14] S. Chelkowski, T. Zuo, and A. D. Bandrauk, Phys. Rev. A **46**, R5342 (1992).
[15] A. D. Bandrauk and H. Z. Lu, Phys. Rev. A **62**, 053406 (2000).
[16] X. Urbain, B. Fabre, V. M. Andrianarijaona, J. Jureta, J. H. Posthumus, A. Saenz, E. Baldit, and C. Cornaggia, Phys. Rev. Lett. **92**, 163004 (2004).
[17] I. Ben-Itzhak, P. Q. Wang, J. F. Xia, A. M. Sayler, M. A. Smith, K. D. Carnes, and B. D. Esry, Phys. Rev. Lett. **95**, 073002 (2005).
[18] J. Hu, K. L. Han, and G. Z. He, Phys. Rev. Lett. **95**, 123001 (2005).
[19] R. F. Lu, P. Y. Zhang, and K. L. Han, Phys. Rev. E **77**, 066701 (2008).
[20] B. Feuerstein and U. Thumm, J. Phys. B **36**, 707 (2003).
[21] A. D. Bandrauk and H. Z. Lu, J. Mol. Struct. (Theochem.) **547**, 97 (2001).
[22] R. F. Lu, C. Y. Xiao, K. M. Deng, and H. P. Wu, Chem. Phys. **382**, 88 (2011).